Statement of significance

The ultrastructural organization of elastic fibers in the transition zone, the interface of the nucleus and annulus of the intervertebral disc, is currently not known. The present research utilized extracellular matrix digestion to visualize the ultrastructural organization of elastic fibers in the transition zone which is crucial to improve our comprehensive understanding of the disc structure and function.

The ultrastructural organization of elastic fibers at the interface of the nucleus and annulus of the intervertebral disc

Javad Tavakoli[1, 2*], Ashish D. Diwan[1, 2, 3], Joanne L. Tipper[1*]

[1]Centre for Health Technologies, School of Biomedical Engineering, Faculty of Engineering and Information Technology, University of Technology Sydney, NSW, Australia

[2]SpineLabs, St George & Sutherland Clinical School, The University of New South Wales,

[3]Spine Service, Department of Orthopaedic Surgery, St George Hospital Campus, NSW, Australia

*Corresponding authors: Prof Joanne L. Tipper (joanne.tipper@uts.edu.au); Dr Javad Tavakoli (javad.tavakoli@uts.edu.au)

Abstract

There has been no study to describe the ultrastructural organization of elastic fibers at the interface of the nucleus pulposus and annulus fibrosus of the intervertebral disc (IVD), a region called the transition zone (TZ). A previously developed digestion technique was optimized to eliminate cells and non-elastin ECM components except for the elastic fibers from the anterolateral (AL) and posterolateral (PL) regions of the TZ in ovine IVDs. Not previously reported, the current study identified a complex elastic fiber network across the TZ for both AL and PL regions. In the AL region, this network consisted of major thick elastic fibers (≈ 1 μm) that were interconnected with delicate (< 200 nm) elastic fibers. While the same ultrastructural organization was observed in the PL region, interestingly the size of the elastic fibers was smaller (< 100 nm) compared to those that were located in the AL region. Quantitative analysis of the elastic fibers revealed significant differences in the size ($p < 0.001$) and the orientation of elastic fibers ($p = 0.001$) between the AL and PL regions, with a higher orientation and larger size of elastic fibers observed in the AL region. The gradual elimination of cells and non-elastin extracellular matrix components identified that elastic fibers in the TZ region in combination with the extracellular matrix created a honeycomb structure that was more compact at the AF interface compared to that located close to the NP. Three different symmetrically organized angles of rotation (0^{o} and $\pm 90^{o}$) were detected for the honeycomb structure at both interfaces, and the structure was significantly orientated at the TZ-AF compared to the TZ-NP interface ($p = 0.003$).

Keywords: Elastic fibers; ultrastructural organization; intervertebral disc; transition zone; Nucleus pulposus; digestion

1. Introduction

The intervertebral disc (IVD) is comprised of three major components, including a central gelatinous nucleus pulposus (NP) and surrounding annulus fibrosus (AF) situated between cartilaginous endplates that interface with the vertebral bodies. The AF consists of collagen fibers (mainly type I) arranged in concentric layers around the NP [1]. This multi-lamellar structure is anchored to the endplates forming a reinforced structure around the NP [2]. The NP is a well hydrated tissue, containing up to 88% water, which forms an amorphous gel with collagen type II and proteoglycans [3].

Microscopically, the main fibrous component of the AF and NP is collagen. A transient gradient from collagen type II from the NP to collagen type I is observed in the AF as one proceeds towards the peripheral AF [4]. Within the AF, parallel arrays of collagen fibers are organized at alternating angles ($\pm 30^{o}$, with respect to the axial axis) in adjacent layers [1]. Compared to the AF, the NP has a lower collagen content with an amorphous structure. Elastic fibers are another fibrous component, distributed across the NP and AF regions, which provide resilience and elasticity to the IVD [5, 6]. The elastic fibers of the IVD have not been well studied. Early studies on IVD structure reported irregular organization of the elastic fibers, therefore the elastic fibers have been considered to play no significant role in the function of the IVD [7-10]. Later light microscopic studies revealed that the distribution and orientation of elastic fibers vary from region to region in the IVD [11-14]. In the AF, elastic fibers are densely concentrated in the inter-lamellar region [15] while long and straight fibers with radial orientation were found in the NP [14]. One study using bovine tail IVD reported that elastic fibers formed a criss-cross pattern at the interface of the NP and AF, a region called the transition zone (TZ) [14]. Although these studies have shown that elastic fibers are abundant in the IVD, they were described to be sparsely dispersed amongst the collagen fibers. Of particular significance, previous studies have failed to identify the

ultrastructural organization of elastic fibers in the IVD, since the elastic fibers are intermingled with other fibrous components and are regularly obscured by the extracellular matrix (ECM). Structural studies based on light microscopic analysis have not revealed the fine architectural details of the elastic fiber network. Recently, a method based on sonication of IVD tissue in sodium hydroxide solution (digestion technique) was developed to eliminate cells and non-elastin ECM components except for elastic fibers making the ultrastructural characterization of IVD elastic fibers possible [16, 17]. We have previously identified that elastic fibers create an orthotropic network in the inter-lamellar matrix within the AF layers. Within the elastic network, both thick and thin fibers are organized at ±45° with the majority of them oriented at 0°[18, 19]. As a key structural feature in the network, elastic fibers of the NP form a network of fibers with different sizes including ultrathin (<50 nm), thin (≈250 nm), and thick (≈ 1 μm) [20]. Even though these important studies clarified a number of unknown characteristics of elastic fibers in the AF and NP, the ultrastructural organization of elastic fibers in the TZ is currently not known and whether elastic fibres in the TZ present a network is yet to be investigated.

While several studies have revealed the connectivity between the NP and endplates [21, 22], to date, the NP has been considered as an insulated entity that is mostly isolated from the AF with unidentifiable boundaries [23-25]. Several studies reported different characteristics of the TZ region by identifying the metabolic activity [26], detecting the structure using a light microscope [14] or a non-destructive imaging technique [27], and reporting on the function, based on the ability of TZ fibers to support transverse load (2-12 N) [28]. To the best of the authors' knowledge, there has been no study to clearly explain the ultrastructural organization of elastic fibers in the TZ which is important to improve our comprehensive understanding of IVD function. Therefore, the aim of the current study was to elucidate the ultrastructural organization of elastic fibers in the TZ in sheep IVD. Sheep IVDs were used in

the current study based on their structural and biochemical similarities to the human IVD [29, 30]. Sheep IVDs are approximately exposed to similar mechanical loads compared to the human IVDs with a loss of notochordal cells in early adulthood was observed in both models [31].

2. Materials and methods

2.1. Sample preparation

Six fresh lumbar sheep spines (>18 months old) were obtained from a local abattoir. The IVDs (Figure 1a) from the L4/L5 level were carefully separated from the vertebrae, wrapped in cling wraps (sealed samples), stored at −20 °C for 24 h. While frozen, blocks of tissue (5× 5 mm) from the anterolateral (AL) and posterolateral (PL) regions of the TZ were isolated. To identify the TZ containing blocks, this process was performed under a microscopic observation (×65 magnification) using a stereomicroscope (SZX10, Olympus). A distance of 5 mm (approximately) from the last layer of the inner AF (IAF) towards the NP was considered to represent the state of the TZ (Figure 1b, denoted by R).

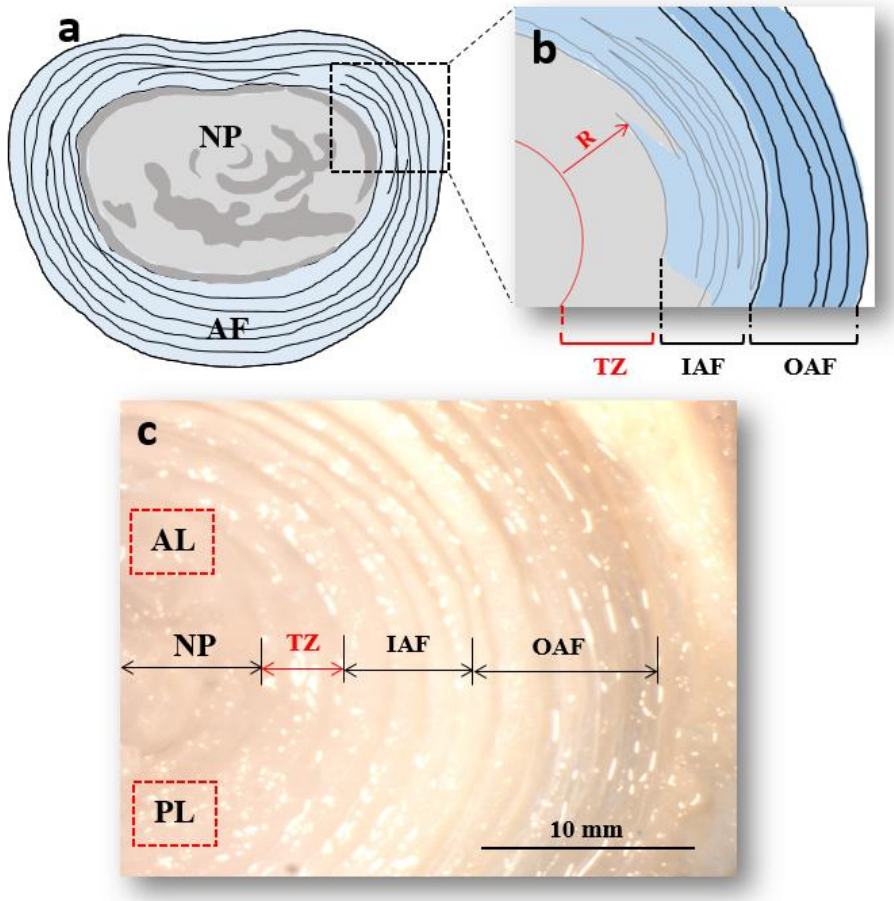

Figure 1- (a) schematic drawing (axial view) of an IVD separated from the vertebrae including the nucleus (NP) and annulus fibrosus (AF) regions. Higher magnification of the anterolateral (AL) region of IVD was presented in (b) to identify the outer annulus fibrosus (OAF), the inner annulus fibrosus (IAF), and the transition zone (TZ) with $R \approx 5$ *mm. (c) The regions of interest (TZ) were denoted by red squares (dotted line) in a microscopic image.*

The region of interest (TZ) was denoted by a red square (dotted line) in a microscopic image that was captured from the anterolateral region of an IVD (Figure 1c). Finally, two axial samples (thickness ≈ 1 mm) from each block were cut, one prepared for sample digestion and the other which served as the control (undigested).

2.2. Sample digestion

To partially digest the sample, for *in situ* isolation of elastic fibers, the previously described method was used [17]. Briefly, samples, harvested from the AL and PL regions of the IVD, were thawed at room temperature and placed in NaOH (0.5 mM) solution, while being sonicated (950 W, probe size 3 mm) for 20-30 min. Following sonication, while still soaked in NaOH solution, samples were placed in an oven (T = 65° C) for 5-10 min. Then samples were washed gently using distilled water, dried in a series of graded ethanol (50 – 100%, step = 10%, for 5 min each), and finally were placed in an oven under vacuum at 37° C and -80 kPa for 1 h. A similar approach for sample preparation was considered at different time points (0, 10, and 30 min) to highlight the efficacy of the digestion process.

2.3. Scanning electron microscopy

All SEM images were captured using Inspect F50 (FEI Company, USA) from the surface of the samples after they were mounted on aluminum stubs using double-sided adhesive tape. Before imaging, all samples were sputter-coated with platinum at 3 nm thickness. For SEM imaging the voltage was set to 5 kV and the distance from the surface of the sample to the beam source kept constant at 18 mm during imaging.

2.4. Quantitative analysis

Open source FIJI software was employed for quantitative using binary images as the input. The results for the geometrical analysis (the size of fibers) were presented as the average of at least five regions of interest in each sample using highly magnified SEM images (> ×110,000) identifying single fibers only. In order to measure the coefficient of directional coherency and distribution of fibers, all SEM images were converted to 8-bit images. Using the FIJI software (segmentation plugin), the SEM images were edited by selecting the automatic threshold with noise threshold, Lambda factor, and minimum leaf size equal to 25, 3, and 87, respectively. The segmented images were further enhanced using Graph Cut

(segmentation plugin) by optimizing parameter foreground bias = 0.5, and smoothness, edge image influence, and edge image decay set to a minimum value. These threshold values were selected to edit SEM images in order to properly distinguish the elastic network apart from the background, which were kept constant for all images during analysis. Circularity, Ferret angle, aspect ratio, and the coherency of directionality were measured using Analyze (measure), and OrientationJ (Dominant Direction) plugins, respectively. To measure the distribution of orientation of fibers (OrientationJ plugin), the Hessian gradient with local window σ = 1 pixels was selected as the structural tensor for fitting the data and all orientations were measured relative to the X-axis (lateral axis of IVD).

2.5. Statistical analysis

One way Anova was conducted (IBM SPSS Statistics for Windows, Version 26, Armonk, NY: IBM Corp.) between different regions (AL: anterolateral and PL: posterolateral), having test variables of fiber orientation, size of fibers, and directional coherency coefficients using an alpha of 0.05. Statistical power analysis, with alpha = 0.05 and sample size = 6, was performed to determine the sample size effect.

3. Results and discussion

Healthy IVDs were utilized in the current study as determined by macroscopic evaluation. While the application of MRI to identify IVD defects is more clinically relevant, our previously published study revealed significant correlations between MRI and macroscopic images to identify IVD damage [32]. The observed power was greater than 0.961 (0.993, 0.998, and 0.961 for the orientation, thickness, and directional coherency coefficient of elastic fibers, respectively), indicating that our proposed sample size was adequate for the main objectives of the current study. To optimize the digestion process, the time of sonication (range 0- 30 min) was adjusted while other parameters including the concentration of sodium

hydroxide, thickness of samples and intensity of the ultrasound remained unchanged. The fibrous components of the TZ were covered by the ECM, making it impossible to identify the organization of elastic fibers using the control samples (Figure 2a). Elimination of the cells and non-elastin ECM components through continuous mild sonication process (figure 2b, c) revealed a progressive improvement in the visualization of elastic fibers in the TZ.

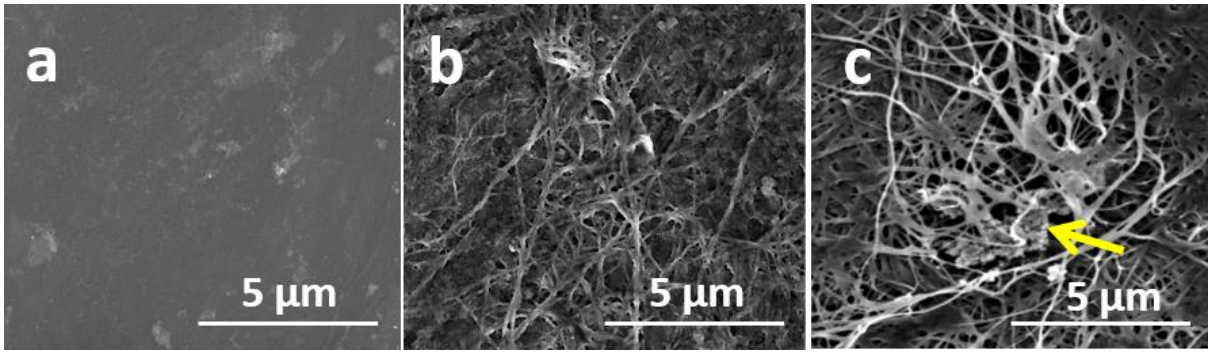

Figure 2- SEM images of the TZ region indicating the effectivity of the digestion process for in situ isolation of elastic fibers at different time points of (a) 0, (b) 10 and (c) 30 min. The elastic fibers in a control sample (t= 0) were obscured by the ECM. The elastic fibers in the partially digested sample (t= 10 min) became almost apparent. The digestion of the samples for 30 min resulted in elimination of cells and non-elastin ECM components except for elastic fibers. The small amounts of debris (ECM) that were remained undigested denoted by a yellow arrow.

Consistent with other studies, the sonication of IVD tissues (in NaOH) that were harvested from the TZ region permits quick *in situ* isolation of elastic fibers, making ultrastructural studies possible using SEM imaging [18, 19]. Previous studies, using histological approaches, have confirmed that the remaining fibrous structure after digestion in NaOH and post-treatment by mild heat were elastic fibers [33-35]. Elastic fibers are hydrophobic and highly insoluble, while collagen fibers are denatured by heat [36]. Sonication increased the rate of digestion, while eliminating the cells and non-elastin ECM components and denatured

collagen fibers resulted in the visualization of elastic fibers. However, occasionally small amounts of debris were observed within the intersection of elastic fibers (denoted by a yellow arrow, Figure 2c). The optimal exposure to sonication during the digestion process preserved the geometery of the elastic fiber network as well as the very delicate elastic fibers usually lost during more aggressive and prolonged digestion procedures.

Not previously reported, the current study identified a dense elastic fiber network across the TZ for both AL and PL regions (Figure 3). This finding suggested that the previous light microscopic observation of crisscross patterns of elastic fibers in the TZ region was just part of the whole and might not reflect the complete ultrastructure [14]. It was found that parallel elastic fibers in the NP that were running towards the AF merged to form an elastic network at the TZ (yellow arrows, Figure 3a). In the AL region, this network consisted of major thick elastic fibers (≈ 1 μm) that were interconnected with delicate (< 200 nm) elastic fibers (Figures 3b, 3c). While the same ultrastructural organization was observed in the PL region, interestingly the size of the elastic fibers was significantly smaller (< 100 nm) compared to those that were located in the AL region (Figure 3d).

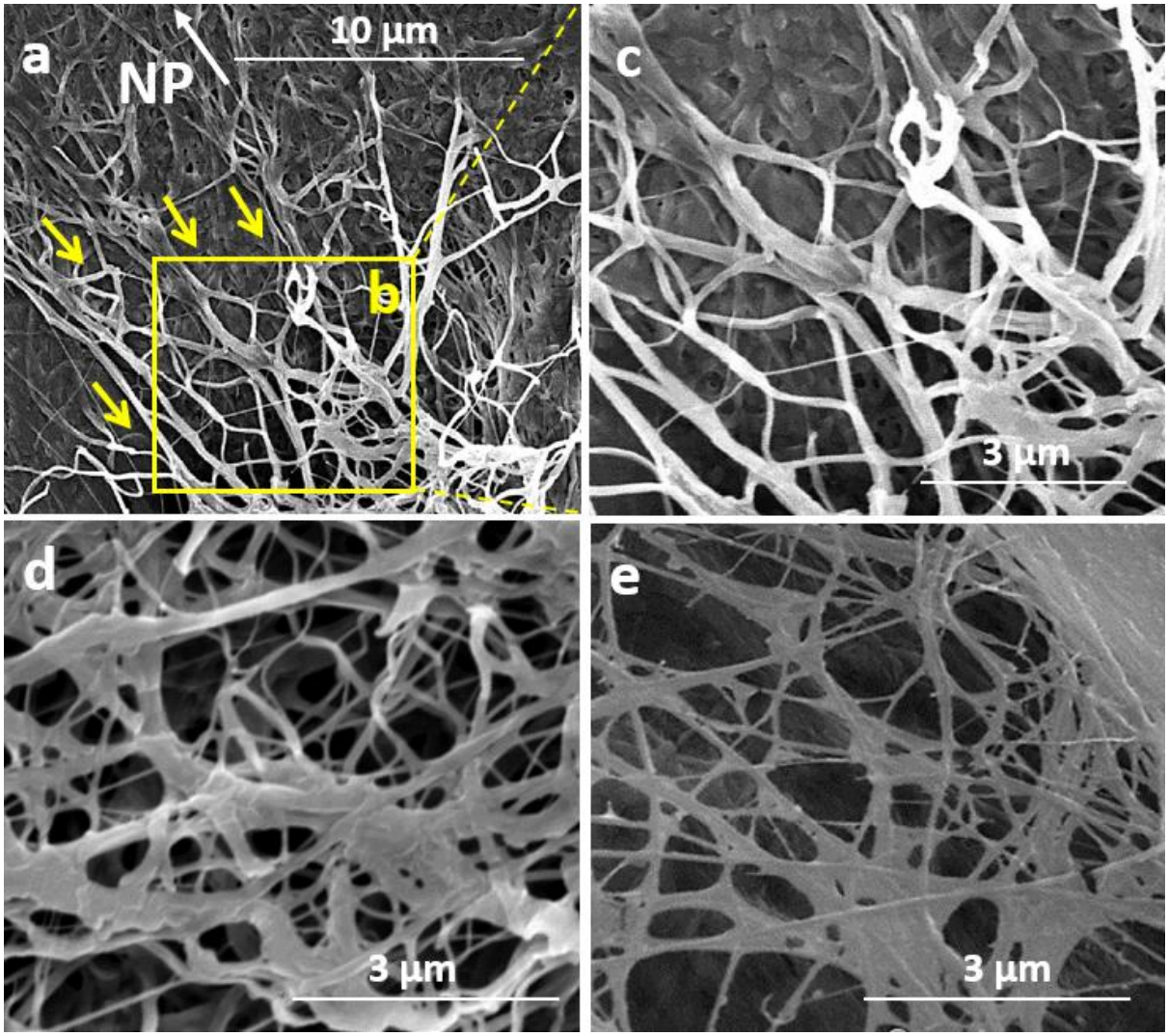

Figure 3- (a) The ultrastructural organization of elastic fibers in the AL region of the TZ in an IVD, with the yellow box denoted by (b) corresponds to the higher magnified image shown in (c) and yellow arrows indicate the almost parallel elastic fibers in the NP merging at the TZ region. The ultrastructural organization of elastic fibers in (d) the AL and (e) the PL region of the TZ in the IVD using different samples to (a).

The observation of a less compact and more delicate elastic network with fiber size < 100 nm for the TZ located in the PL, compared to those in the AL region, may explain why the PL region is more susceptible to damage during herniation. Clinical observations and in-vitro experiments using animal IVDs to develop herniation have revealed that herniation more frequently occurs in the PL, while no herniation was found in the AL region [37, 38]. A

detailed mechanical examination is essential to thoroughly understand the structure-function relationship of elastic fibers and characterize their properties at the TZ, including how stress is distributed throughout the elastic network. One study indicated that the TZ region can support an average tensile load equal to 5 N; however, the incorporation of elastic fibers is not clear [28]. Nevertheless, based on the structural differences for the elastic network in the AL and PL regions, the likely mechanical role of the networks can be speculated. Extensible elastic fibers are likely to assist TZ tissue in returning to its original shape after deformation. While collagen fibers are known to control the overall stiffness of IVD tissue, parallel alignment and cross-connectivity between collagen bundles and the elastic network in the TZ may play an important role in the structural integrity of the IVD tissue to further control tissue deformation and affecting the overall mechanical properties. The delicate elastic network in the PL region is less likely to fully recover after being exposed to high forces during herniation. In contrast, a dense elastic network consisting of elastic fibers with different sizes and shapes in the AL region are more likely to survive the high loads generated during herniation. The observation of a thicker elastic fiber network in the AL region of the TZ is also consistent with a study revealed that the inner AF was stiffer in the AL compared to the PL region [39].

Within both regions of interest (AL and PL), the frequently occurring structural features (an elastic network comprising different size and shape of elastic fibers) were observed (Figures 4 and 5) with a more dense network with bigger elastic fibers available in the AL, compared to the PL region.

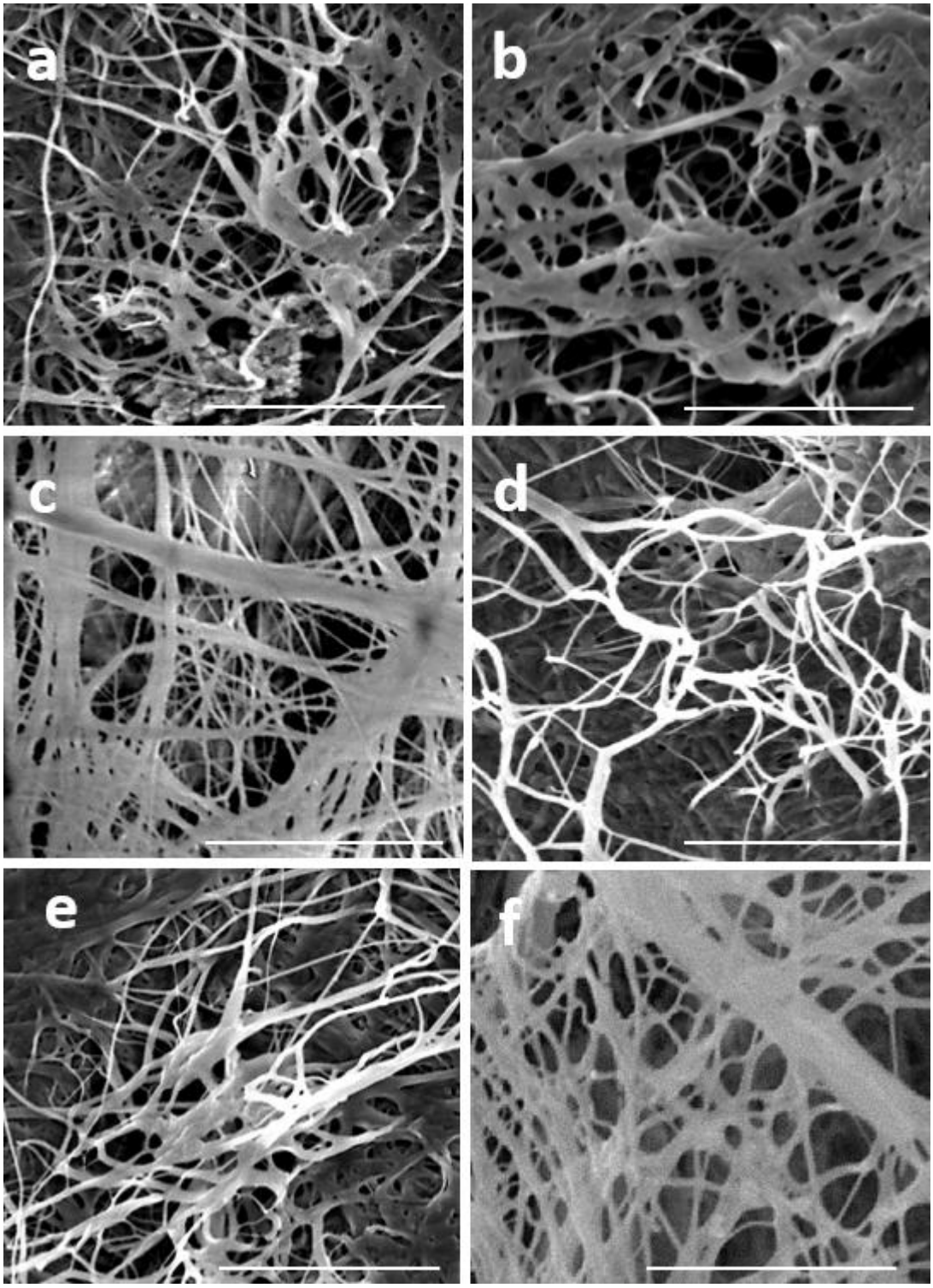

Figure 4 – (a - f) Frequently occurring features of an elastic network in the anterolateral region (AL) of the TZ across all six IVD samples (digested) at 5µm scale bar.

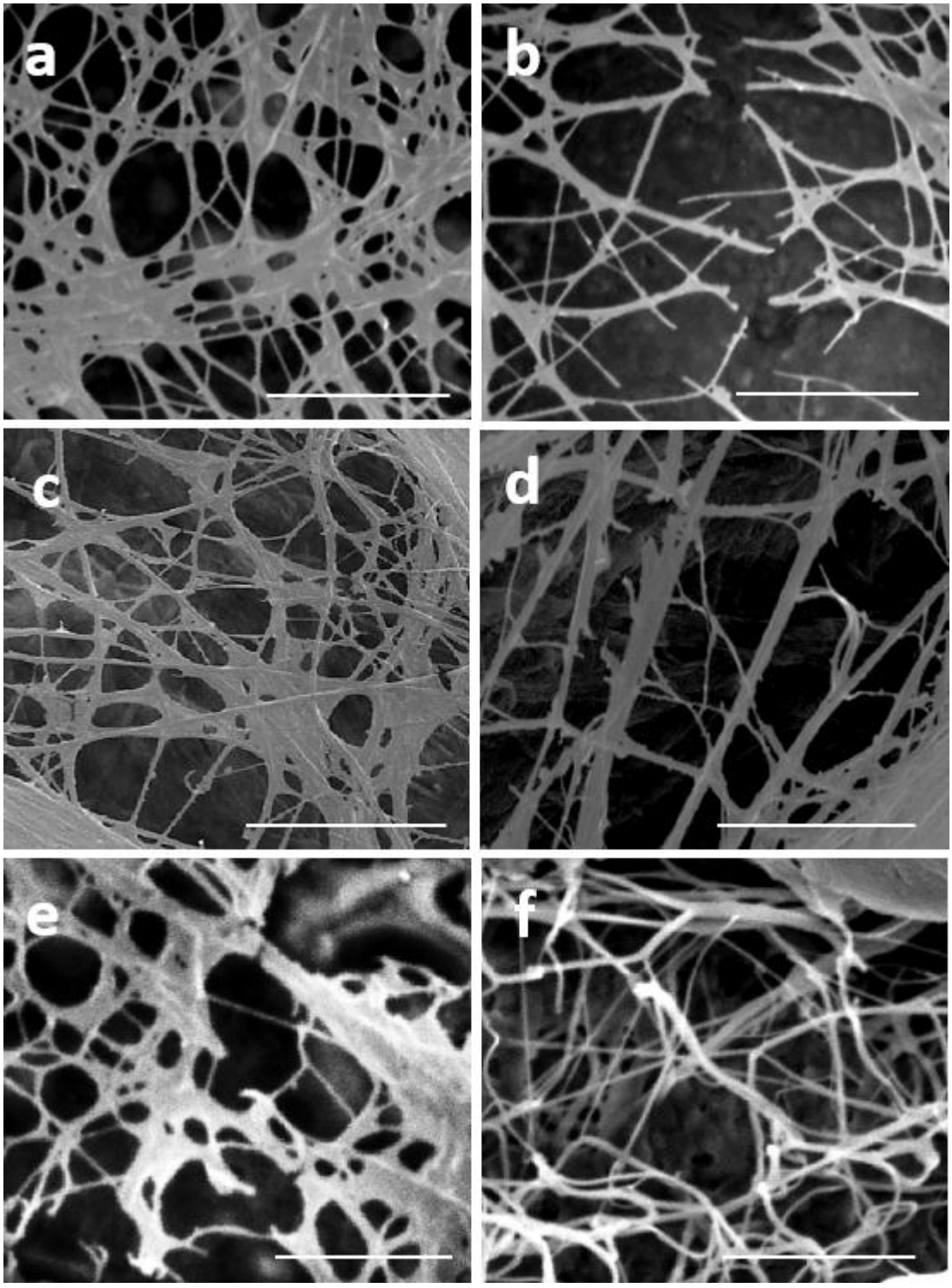

Figure 5 – (a – f) Frequently occurring features of an elastic network in the posterolateral region (PL) of the TZ across all six IVD six samples (digested) at 5µm scale bar.

Quantitative analysis of the elastic fibers revealed significant differences in the size ($p < 0.001$) and the orientation of elastic fibers ($p = 0.001$) between the AL and PL regions, with a higher orientation and larger size of elastic fibers observed in the AL region (Figure 6).

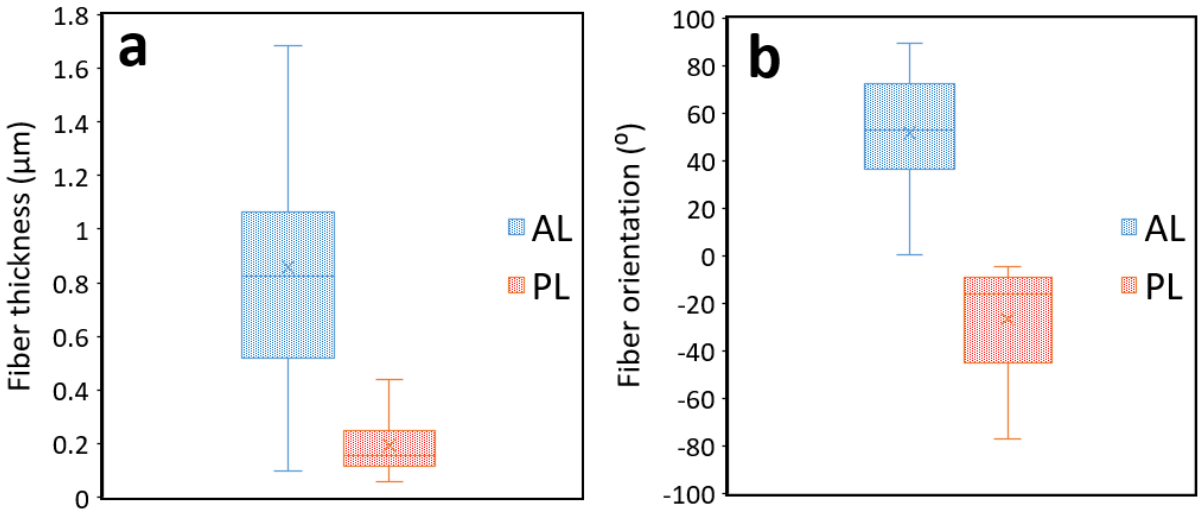

Figure 6- Box plots representing (a) the thickness and (b) the orientation of the elastic fibers in the anterolateral (AL) and posterolateral (PL) regions of the TZ.

Mean (± std) values for the size of elastic fibers were equal to 0.89 (0.10) and 0.19 (0.08) µm for the AL and PL regions, respectively. Also, a positive and higher orientation equal to 51.8° (26.7°) was observed for the elastic fibers located in the AL, compared to the PL region which had a negative and lower orientation of -27.2° (23.9°). The orientation of elastic fibers for both regions was measured relative to the x-axis with the positive and negative signs indicating CW and CCW orientations for the elastic fibers, respectively.

While the findings of the current study revealed different ultrastructural organization (size and orientation) of the elastic network between the AN and PL of the TZ region, more studies are required to identify similarities in the lateral sections (right vs left) of the NP. By analyzing the distribution of fiber orientation to compare the AL with the PL region, three different symmetrically organized angles of rotation were detected in both the regions (Figure 7) occurring at 0° and ±90° . In the AL region, the average number of fibers was 1664.4,

2171.4, and 1709.2 at -90º , 0º , and +90º , respectively. Also, it was determined that the average number of fibers in the PL region was lower than those located in the AL region with 1190.3, 1889.4, and 1220.9 at -90º , 0º , and +90º , respectively.

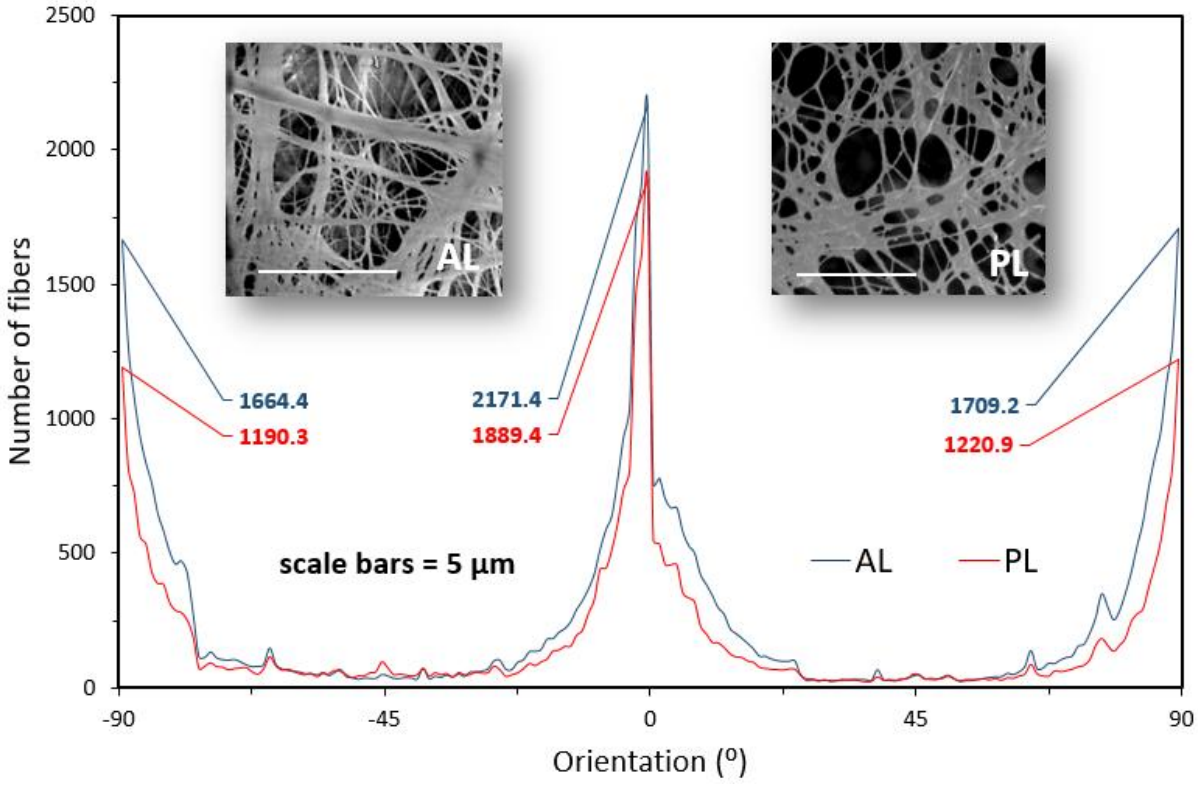

Figure 7- Elastic fiber orientation versus the number of fibers in the AL (blue line) and PL (red line) of the TZ region.

Since a delicate network of elastic fibers was found in the PL region and in order to assure that the effect of optimum digestion on the ultrastructural organization of elastic fibers in the PL region was minimized, five more samples were exposed to a lower digestion time (15 min, reduced-time digestion; Figure 8 & supplementary 1). Our further detailed analysis, comparing the optimum and reduced-time digested samples, showed similar structural features amongst all samples. Two different shape factors of circularity and aspect ratio and ferret angle were extracted from images to compare the structural features. Shape factors are dimensionless quantities that numerically describe the structure of the region of interest and

reflect its degree of deviation from an ideal shape. Using segmented images, negligible differences were found for circularity (0.783 and 0.782), ferret angle (138.13^{o} and 138.55^{o}) and aspect ratio (1.11 and 1.13) of the segments between digested and reduced-time digested samples, indicating that the impact of digestion was minimal. The values were reported for optimum and reduced-time digested samples, respectively. However, interesting ultrastructural features for the elastic fibers were detected through a detailed observation. Firstly, based on the SEM images that were captured using reduced-time digested samples (Figure 8), it was observed that the combination of the ECM and elastic fibers network creates a honeycomb structure in the TZ region. The formation of ice crystals in a biological tissue during the freezing process may cause structural changes leading to the creation of multiple holes, known as the "swiss cheese" effect. The methodology employed in the current study which did not involve snap freezing of the tissue was a limitation towards minimizing the ice crystal formation. However, evidence to support the hypothesis that the honeycomb structure was formed as a result of digestion and was not an artifact of the freezing procedure was apparent from observation of the presence of similar structures in partially digested fresh tissue (Supplementary information 2). In addition, the observation of a honeycomb structure in the current study at the interface of the NP and AF, was consistent with light microscopic results reported by Yu et al., who observed a criss-cross pattern of the elastic fibers at the NP-AF junction in bovine tissue [14]. Secondly, it was observed that the elastic fibers in the TZ region create bigger fenestrations and form a less dense network when moving towards the NP (Figures 8a, b, d, and f), compared to those located close to the AF layers. For the TZ region which is close to the AF layers, the elastic network is more compact creating small fenestrations (Figures 8a, c, and e). The observation of a highly compact structure for the elastic fibers at the interface of TZ and AF regions is consistent with other studies reported a high density of elastic fibers in the interlamellar region [11, 15, 18, 19]. While more

mechanical studies are required, the change in stiffness between the AF and NP may explain the structural change for the elastic fibers seen at the AF-NP interface. This structural change was formed at the early stage of the fetus or shaped as a consequence of loading over time is yet to investigate.

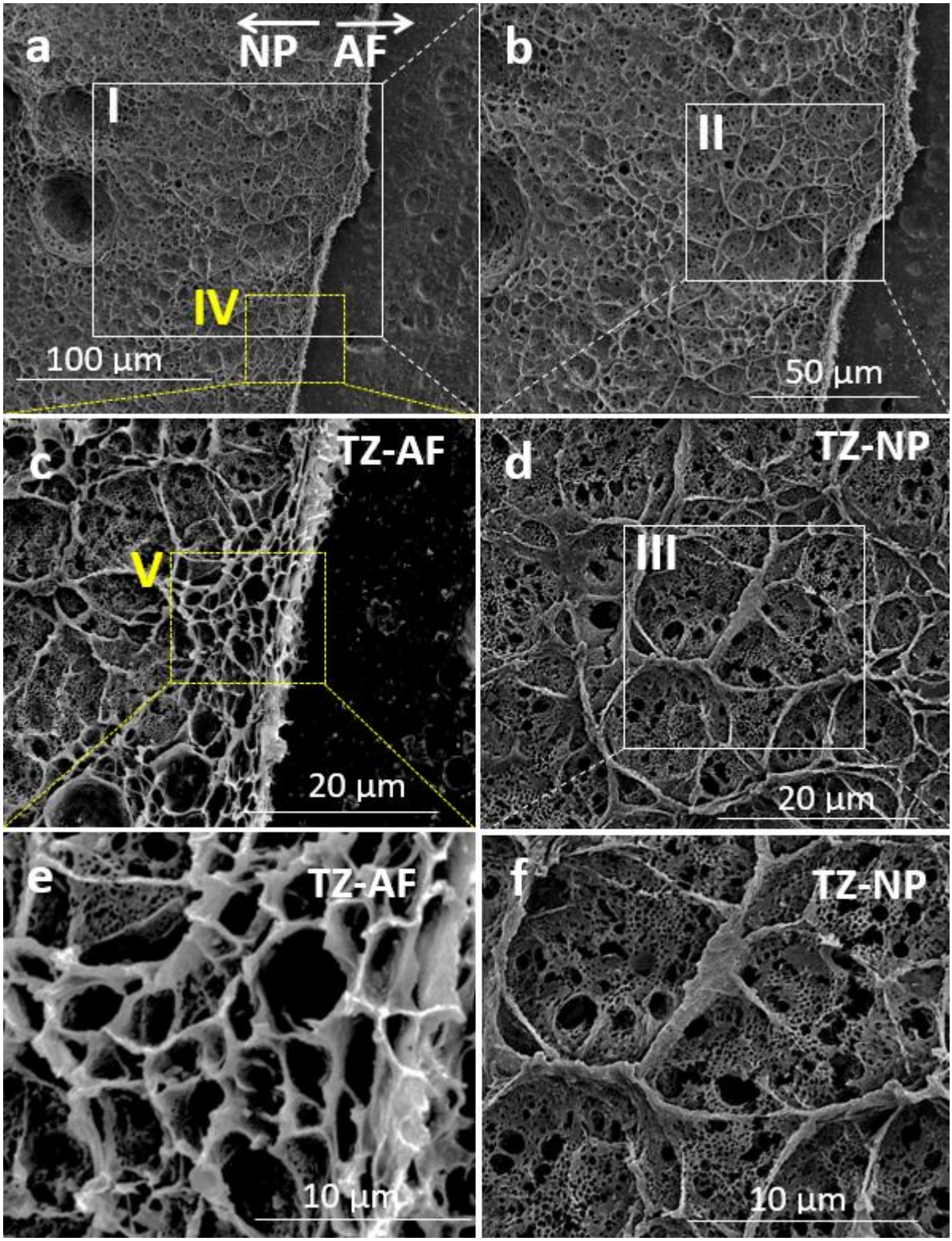

Figure 8- Remnants of the undigested ECM in the reduced-time digested samples revealed a honeycomb structure for the elastic fibers in the TZ region. The SEM images that were captured under different magnifications reported two different structural organizations for

the elastic fibers in the TZ region. When SEM images of the TZ region were captured close to the NP (b, d, and f) a less compact network was observed compared to those that were seen at the TZ-AF interface (c, e). The white boxes denoted by I, II, and III correspond to higher magnified b, d, and f, respectively. Similarly, the yellow boxes denoted by IV and V correspond to high magnification images in c and e, respectively.

Similar structural features for the elastic fiber network in the TZ region were frequently observed amongst all samples (Figures 9a - h). By analyzing the distribution of fiber orientation, three different symmetrically organized angles of rotation were detected in both the interface of the TZ with the AF (TZ-AF) and NP (TZ towards the NP; TZ-NP) regions (Figure 9i) occurring at 0^{o} and $\pm 90^{o}$. In the TZ-AF region, the average number of fibers was 4137, 4200, and 4375 at -90^{o}, 0^{o}, and $+90^{o}$, respectively. Also, it was determined that the average number of fibers in the TZ-NP region was lower than those located in the TZ-AF region with 3079, 3405, and 3099 at -90^{o}, 0^{o}, and $+90^{o}$, respectively. The visualization of the TZ elastic network under high magnification revealed that the density of elastic fibers in the TZ was higher compared to those located in the AF region while their distributions of orientation were similar [18, 19]. The results of the distribution of fibers may be affected by the remnant of the undigested ECM and therefore image properties (brightness, contrast, threshold…) should be adjusted carefully to minimize the effect of the non-elastic component on the measurement of elastic fibers orientation.

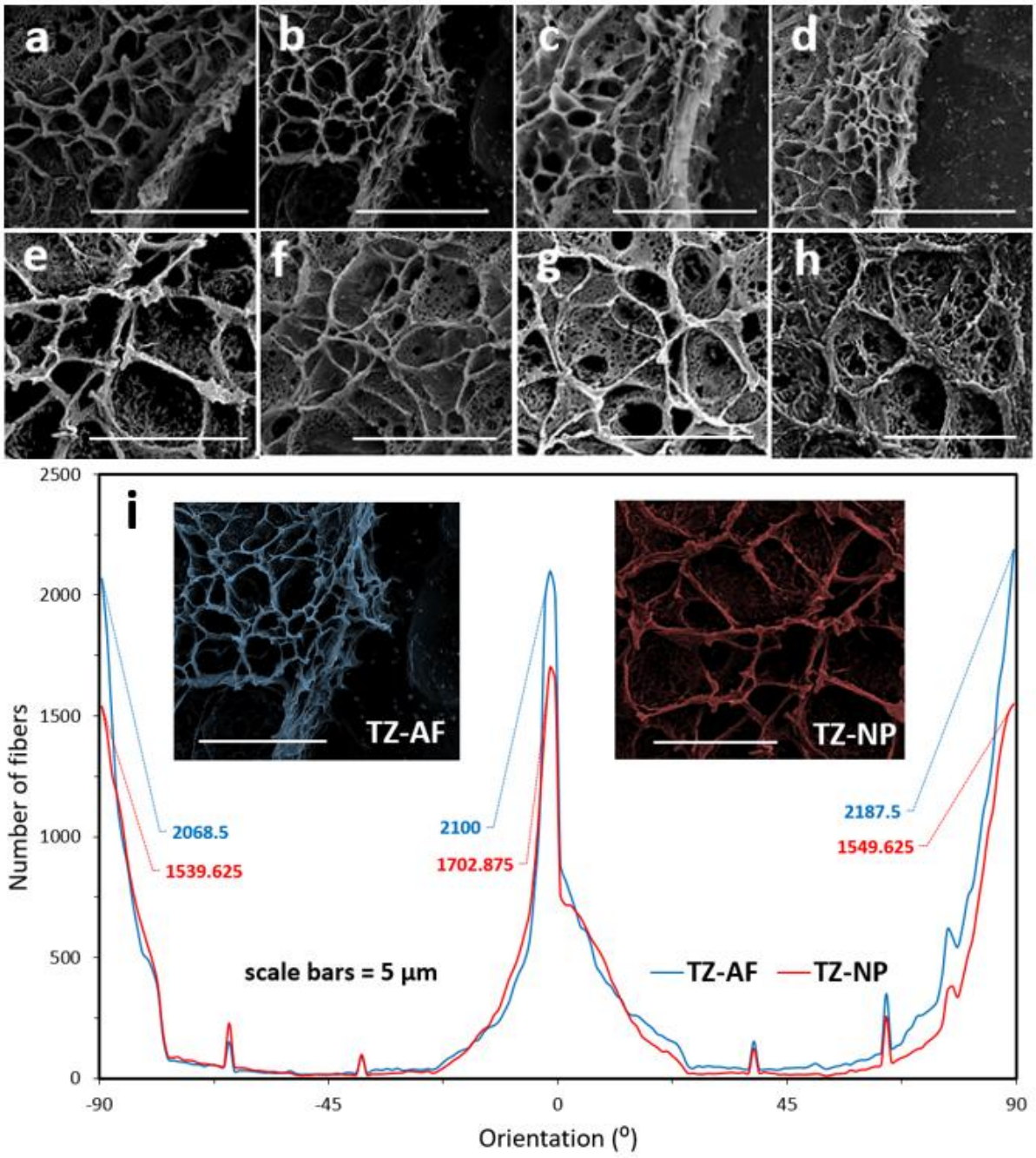

Figure 9- (a - h) Frequently occurring features of an elastic network with different compactness in the posterolateral region across four samples (reduced-time digested) indicating two regions of interests (a – d) TZ-AF and (e – h) TZ-NP. (i) Elastic fiber orientation versus the number of fibers in the TZ region at the AF interface (blue line) and close to the NP (red line), relative to the x-axis. The scale bars are 5 µm.

The quantitative analysis for the directional coherency coefficient is presented in Table 1. While a value equal to zero for the coherency coefficient denotes no preferential orientation, a value close to 1 indicates a strongly coherent orientation of the local fibers.

Table 1- Directional coherency coefficient for elastic fibers in the posterolateral TZ region

Sample	**Region of interest**	
	TZ-NP	TZ-AF
Sample 1	0.017	0.065
Sample 2	0.054	0.073
Sample 3	0.047	0.096
Sample 4	0.055	0.102
Sample 5	0.036	0.084
Mean ± std	**0.042 ± 0.015**	**0.084 ± .015**

Mean (±std) values for directional coherency coefficients of elastic fibers were equal to 0.042 (0.015) and 0.084 (0.015) for TZ-NP and TZ-AF regions, respectively. A significant difference for the directional coherency coefficients was defined between these regions ($p = 0.003$), indicating that the elastic fibers at the TZ-AF interface are more orientated compared to those located in the TZ-NP region. However, with the overall directional coherency coefficients $<<1$, it appears that elastic fibers in the TZ region have no preferential orientation.

The results of the current study (Figure 10) may support further studies to mechanistically investigate the mechanical properties of the elastic fibers in the TZ region. Future approaches may include the execution of mechanical experiments in both shear and tensile directions of loading, using the control and digested samples, to identify the impact of elastic fibers and the ECM on the structural integrity of the TZ region. This strategy was successfully applied to the interlamellar matrix of the AF using ovine IVDs and identified a number of novel

mechanical properties of the elastic fibers. It was reported that the elastic fiber network in the interlamellar matrix exhibited nonlinear elastic behavior with a higher capability to absorb energy at slow strain rates, due to the presence of intra-fibrillar water in the elastic fiber network after digestion.

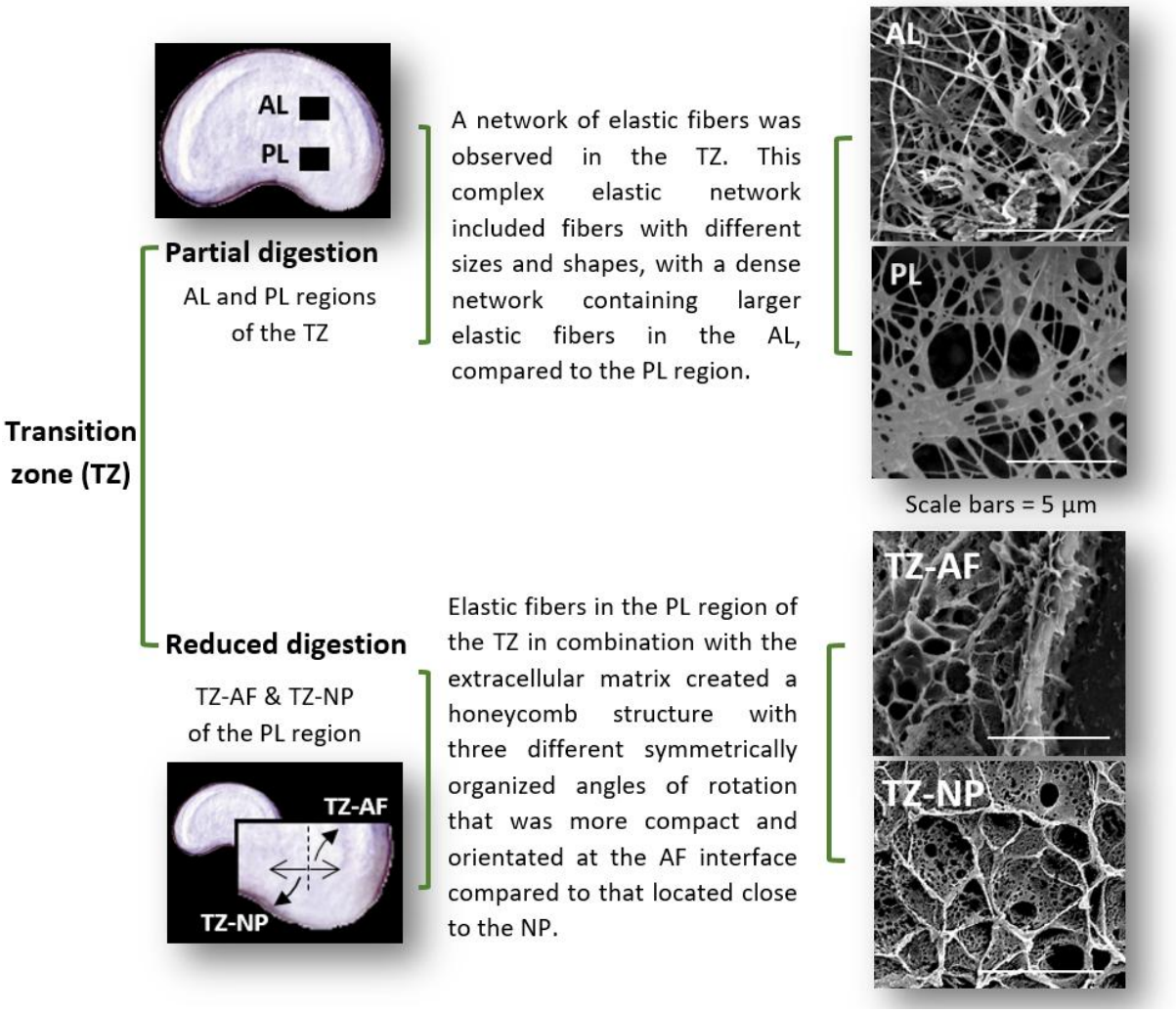

Figure 10- Summary of findings to describe the ultrastructure organization of elastic fibers in the TZ region of the IVD.

This strategy was successfully applied to the interlamellar matrix of the AF using ovine IVDs and identified a number of novel mechanical properties of the elastic fibers. It was reported that the elastic fiber network in the interlamellar matrix exhibited nonlinear elastic behavior with a higher capability to absorb energy at slow strain rates, due to the presence of

intra-fibrillar water in the elastic fiber network after digestion. Also, it was revealed that the elastic fibers in the interlamellar matrix can uptake a significantly higher failure force in tension compared to shear loading [40, 41]. Application of a similar mechanical testing strategy to identify the mechanical properties of the elastic fibers in the TZ region will provide important data to develop more clinically relevant computational models incorporating the role of elastic fibers and enhance the available methods for investigating IVD microstructural deformation [42-44]. In addition, the present structural data may be employed to create an effective IVD structural model to ultimately contribute to the development of more reliable tissue-engineered scaffolds for IVD regeneration. The lack of engineered tissues recapitulating the intrinsic complexity of the IVD structure is a severe limitation toward re-establishing function through regenerative therapies. Simple injectable hydrogels that are currently used as tissue-engineered scaffolds for regeneration of the IVD do no restore native structure (essentially at the micro and sub-micro level) and function, thereby exhibiting limited efficacy [45-49].

In the present study, by implementing a partial digestion method to eliminate cells and non-elastin ECM components from ovine IVDs, significant gaps in understanding of the TZ ultrastructure were addressed and the data generated will contribute to multidisciplinary ultrastructure-function studies in the future. However, the use of human IVDs is more clinically relevant. Since the TZ structure may vary with age, degeneration, and disease, further investigations must be performed to address these questions. Our previously published studies have revealed that the impact of the digestion process on the structural features was minimal (< 2° changes in the major angle of fiber orientation) [16]. However, damage to the tissue during sample preparation has to be carefully considered for the visualization of elastic fibers, specifically in tissues containing loose and sparse hierarchical assembly of fibers. A detailed examination using serial adjacent samples harvested from different cutting planes

(oblique and axial) may also assist to elucidate a 3D model of elastic fiber networks in the TZ region.

4. Conclusion

The aim of the current study was to visualize the ultrastructural organization of elastic fibers in the TZ of IVD and identify their structural characteristics. Not previously reported, the result of this study identified a complex elastic network including fibers with different sizes and shapes with a more dense network with bigger elastic fibers available in the AL, compared to the PL region. This network consisted of major thick elastic fibers (≈ 1 μm) that were interconnected with delicate (< 200 nm) elastic fibers. In addition, a significantly higher orientation of elastic fibers was observed in the AL compared to the PL region. It was revealed that the density of the elastic network in the TZ region is higher than those that were observed for the AF region including the inter- and intra-lamellar regions. The gradual elimination of cells and non-elastin ECM components identified that elastic fibers in the TZ region in combination with the ECM created a honeycomb structure that was more compact and orientated at the AF interface compared to that located close to the NP. However, with the overall directional coherency coefficients <<1, it appears that elastic fibers in the TZ region have no preferential orientation. Three different symmetrically organized angles of rotation were detected for the honeycomb structure at both interfaces, and the structure was significantly orientated at the TZ-AF compared to the TZ-NP interface.

Acknowledgments

Javad Tavakoli is grateful for the support of the University of Technology Sydney (UTS) with a Chancellor's Postdoctoral Research Fellowship (CPDRF) for the research work.

Conflict of interest

The authors declare no conflict of interest.

5. Reference

[1] J.J. Cassidy, A. Hiltner, E. Baer, Hierarchical structure of the intervertebral disc, Connect Tissue Res 23(1) (1989) 75-88.

[2] S.A. Rodrigues, K.R. Wade, A. Thambyah, N.D. Broom, Micromechanics of annulus-end plate integration in the intervertebral disc, Spine J 12(2) (2012) 143-50.

[3] P. Adams, D. Eyre, H. Muir, Biochemical aspects of development and ageing of human lumbar intervertebral discs, Rheumatology 16(1) (1977) 22-29.

[4] D.R. Eyre, H. Muir, Quantitative analysis of types I and II collagens in human intervertebral discs at various ages, Biochimica et Biophysica Acta (BBA)-Protein Structure 492(1) (1977) 29-42.

[5] J. Yu, Elastic tissues of the intervertebral disc, Portland Press Ltd., 2002.

[6] L.J. Smith, S. Byers, J.J. Costi, N.L. Fazzalari, Elastic fibers enhance the mechanical integrity of the human lumbar anulus fibrosus in the radial direction, Annals of biomedical engineering 36(2) (2008) 214-223.

[7] J. Buckwalter, R. Cooper, J. Maynard, Elastic fibers in human intervertebral discs, JBJS 58(1) (1976) 73-76.

[8] E.F. Johnson, R.W. Caldwell, H.E. Berryman, A. Miller, K. Chetty, Elastic fibers in the anulus fibrosus of the dog intervertebral disc, Cells Tissues Organs 118(4) (1984) 238-242.

[9] M. Humzah, R. Soames, Human intervertebral disc: structure and function, The Anatomical Record 220(4) (1988) 337-356.

[10] E.F. Johnson, H. Berryman, R. Mitchell, W.B. Wood, Elastic fibres in the anulus fibrosus of the adult human lumbar intervertebral disc. A preliminary report, J Anat 143 (1985) 57-63.

[11] L.J. Smith, N.L. Fazzalari, Regional variations in the density and arrangement of elastic fibres in the anulus fibrosus of the human lumbar disc, J Anat 209(3) (2006) 359-367.

[12] L.J. Smith, N.L. Fazzalari, The elastic fibre network of the human lumbar anulus fibrosus: architecture, mechanical function and potential role in the progression of intervertebral disc degeneration, European Spine Journal 18(4) (2009) 439-448.

[13] J. Yu, U. Tirlapur, J. Fairbank, P. Handford, S. Roberts, C. Winlove, Z. Cui, J. Urban, Microfibrils, elastin fibres and collagen fibres in the human intervertebral disc and bovine tail disc, J Anat 210 (2007) 460-71.

[14] J. Yu, P.C. Winlove, S. Roberts, J.P.G. Urban, Elastic fibre organization in the intervertebral discs of the bovine tail, J Anat 201(6) (2002) 465-475.

[15] J. Tavakoli, D.M. Elliott, J.J. Costi, Structure and mechanical function of the inter-lamellar matrix of the annulus fibrosus in the disc, Journal of Orthopaedic Research 34(8) (2016) 1307-1315.

[16] J. Tavakoli, J.J. Costi, Development of a rapid matrix digestion technique for ultrastructural analysis of elastic fibers in the intervertebral disc, Journal of the mechanical behavior of biomedical materials 71 (2017) 175-183.

[17] J. Tavakoli, J.J. Costi, A method for visualization and isolation of elastic fibres in annulus fibrosus of the disc, Materials Science and Engineering: C 93 (2018) 299-304.

[18] J. Tavakoli, J.J. Costi, Ultrastructural organization of elastic fibres in the partition boundaries of the annulus fibrosus within the intervertebral disc, Acta Biomaterialia 68 (2018) 67-77.

[19] J. Tavakoli, D.M. Elliott, J.J. Costi, The ultra-structural organization of the elastic network in the intra- and inter-lamellar matrix of the intervertebral disc, Acta Biomaterialia 58 (2017) 269-277.

[20] J. Tavakoli, A.D. Diwan, J.L. Tipper, Elastic fibers: The missing key to improve engineering concepts for reconstruction of the Nucleus Pulposus in the intervertebral disc, Acta Biomaterialia (2020).

[21] K.R. Wade, P.A. Robertson, N.D. Broom, On how nucleus-endplate integration is achieved at the fibrillar level in the ovine lumbar disc, J Anat 221(1) (2012) 39-46.

[22] K.R. Wade, P.A. Robertson, N.D. Broom, A fresh look at the nucleus-endplate region: new evidence for significant structural integration, European Spine Journal 20(8) (2011) 1225-1232.

[23] S.E. Gullbrand, D.H. Kim, E. Bonnevie, B.G. Ashinsky, L.J. Smith, D.M. Elliott, R.L. Mauck, H.E. Smith, Towards the scale up of tissue engineered intervertebral discs for clinical application, Acta Biomaterialia 70 (2018) 154-164.
[24] M. D'Este, D. Eglin, M. Alini, Lessons to be learned and future directions for intervertebral disc biomaterials, Acta Biomaterialia 78 (2018) 13-22.
[25] J. Urban, S. Roberts, J. Ralphs, The nucleus of the intervertebral disc from development to degeneration, American Zoologist 40(1) (2000) 53-061.
[26] T. Taylor, P. Ghosh, G. Bushell, The contribution of the intervertebral disk to the scoliotic deformity, Clinical orthopaedics and related research (156) (1981) 79-90.
[27] M. Sharabi, K.R. Wade, F. Galbusera, V. Rasche, R. Haj-Ali, H.-J. Wilke, Three-dimensional microstructural reconstruction of the ovine intervertebral disc using ultrahigh field MRI, The Spine Journal 18(11) (2018) 2119-2127.
[28] K.R. Wade, P.A. Robertson, N.D. Broom, On the extent and nature of nucleus-annulus integration, Spine 37(21) (2012) 1826-1833.
[29] G.D. O'Connell, E.J. Vresilovic, D.M. Elliott, Comparison of animals used in disc research to human lumbar disc geometry, Spine 32(3) (2007) 328-333.
[30] H.-J. Wilke, A. Kettler, L.E. Claes, Are sheep spines a valid biomechanical model for human spines?, Spine 22(20) (1997) 2365-2374.
[31] C. Daly, P. Ghosh, G. Jenkin, D. Oehme, T. Goldschlager, A Review of Animal Models of Intervertebral Disc Degeneration: Pathophysiology, Regeneration, and Translation to the Clinic, Biomed Res Int 2016 (2016) 5952165-5952165.
[32] D.B. Amin, J. Tavakoli, B.J. Freeman, J.J. Costi, Mechanisms of Failure Following Simulated Repetitive Lifting: A Clinically Relevant Biomechanical Cadaveric Study, Spine 45(6) (2020) 357-367.
[33] R.S. Crissman, L.A. Pakulski, A Rapid Digestive Technique to Expose Networks of Vascular Elastic Fibers for Sem Observation, Stain Technology 59(3) (1984) 171-180.
[34] R.S. Crissman, J.N. Ross Jr, T. Davis, Scanning electron microscopy of an elastic fiber network which forms the internal elastic lamina in canine saphenous vein, The Anatomical Record 198(4) (1980) 581-593.
[35] T. Ushiki, Collagen fibers, reticular fibers and elastic fibers. A comprehensive understanding from a morphological viewpoint, Archives of histology and cytology 65(2) (2002) 109-126.
[36] N. Wright, J. Humphrey, Denaturation of collagen via heating: an irreversible rate process, Annual review of biomedical engineering 4(1) (2002) 109-128.
[37] J. Tavakoli, D.B. Amin, B.J. Freeman, J.J. Costi, The biomechanics of the inter-lamellar matrix and the lamellae during progression to lumbar disc herniation: which is the weakest structure?, Annals of biomedical engineering 46(9) (2018) 1280-1291.
[38] S. Rajasekaran, N. Bajaj, V. Tubaki, R.M. Kanna, A.P. Shetty, ISSLS Prize Winner: The Anatomy of Failure in Lumbar Disc HerniationAn In Vivo, Multimodal, Prospective Study of 181 Subjects, Spine 38(17) (2013) 1491-1500.
[39] G.A. Holzapfel, C. Schulze-Bauer, G. Feigl, P. Regitnig, Single lamellar mechanics of the human lumbar anulus fibrosus, Biomechanics and modeling in mechanobiology 3(3) (2005) 125-140.
[40] J. Tavakoli, J.J. Costi, New insights into the viscoelastic and failure mechanical properties of the elastic fiber network of the inter-lamellar matrix in the annulus fibrosus of the disc, Acta Biomaterialia 77 (2018) 292-300.
[41] J. Tavakoli, J.J. Costi, New findings confirm the viscoelastic behaviour of the inter-lamellar matrix of the disc annulus fibrosus in radial and circumferential directions of loading, Acta Biomaterialia 71 (2018) 411-419.
[42] C.M. Disney, A. Eckersley, J.C. McConnell, H. Geng, A.J. Bodey, J.A. Hoyland, P.D. Lee, M.J. Sherratt, B.K. Bay, Synchrotron tomography of intervertebral disc deformation quantified by digital volume correlation reveals microstructural influence on strain patterns, Acta Biomaterialia 92 (2019) 290-304.

[43] C. Vergari, J. Mansfield, J.R. Meakin, P.C. Winlove, Lamellar and fibre bundle mechanics of the annulus fibrosus in bovine intervertebral disc, Acta Biomaterialia 37 (2016) 14-20.
[44] K. Kandil, F. Zaïri, A. Derrouiche, T. Messager, F. Zaïri, Interlamellar-induced time-dependent response of intervertebral disc annulus: A microstructure-based chemo-viscoelastic model, Acta Biomaterialia 100 (2019) 75-91.
[45] H. Ishiguro, T. Kaito, S. Yarimitsu, K. Hashimoto, R. Okada, J. Kushioka, R. Chijimatsu, S. Takenaka, T. Makino, Y. Sakai, Y. Moriguchi, S. Otsuru, D.A. Hart, H. Fujie, N. Nakamura, H. Yoshikawa, Intervertebral disc regeneration with an adipose mesenchymal stem cell-derived tissue-engineered construct in a rat nucleotomy model, Acta Biomaterialia 87 (2019) 118-129.
[46] S.E. Gullbrand, T.P. Schaer, P. Agarwal, J.R. Bendigo, G.R. Dodge, W. Chen, D.M. Elliott, R.L. Mauck, N.R. Malhotra, L.J. Smith, Translation of an injectable triple-interpenetrating-network hydrogel for intervertebral disc regeneration in a goat model, Acta Biomaterialia 60 (2017) 201-209.
[47] H. Zhang, S. Yu, X. Zhao, Z. Mao, C. Gao, Stromal cell-derived factor-1α-encapsulated albumin/heparin nanoparticles for induced stem cell migration and intervertebral disc regeneration in vivo, Acta Biomaterialia 72 (2018) 217-227.
[48] C. Ligorio, M. Zhou, J.K. Wychowaniec, X. Zhu, C. Bartlam, A.F. Miller, A. Vijayaraghavan, J.A. Hoyland, A. Saiani, Graphene oxide containing self-assembling peptide hybrid hydrogels as a potential 3D injectable cell delivery platform for intervertebral disc repair applications, Acta Biomaterialia 92 (2019) 92-103.
[49] A.A. Thorpe, G. Dougill, L. Vickers, N.D. Reeves, C. Sammon, G. Cooper, C.L. Le Maitre, Thermally triggered hydrogel injection into bovine intervertebral disc tissue explants induces differentiation of mesenchymal stem cells and restores mechanical function, Acta Biomaterialia 54 (2017) 212-226.